Buletinul Ştiinţific al Universităţii "Politehnica" din Timişoara

Seria ELECTRONICĂ şi TELECOMUNICAŢII
TRANSACTIONS on ELECTRONICS and COMMUNICATIONS

Tom 53(67), Fascicola 2, 2008

Hyperanalytic Wavelet-based Watermarking

Corina Nafornita, Alexandru Isar[1]

Abstract – In this paper we present a new technique for watermarking in the hyperanalytic wavelet domain. This has the advantage of better directional selectivity and shift invariance compared to the classical wavelet filter. The watermark is inserted into all levels of decomposition using a perceptual mask conceived by the authors. We compare this technique with two systems in the DWT domain, and show its superiority. We study the resistance of the three watermarking systems against various signal processing attacks and the recently proposed local desynchronization attack (DA), namely the local permutation with cancelation and duplication (LPCD) DAs. For LPCD DA, simulation results show that while the attacked watermarked images are visually similar with the watermarked ones, the correlation or similarly the Peak Signal-to-Noise ratio, between them is decreased, indicating the effectiveness of the attack. All three methods successfully detect the watermark, with superiority from the hyperanalytic wavelet domain. This leads to the conclusion that the Hyperanalytic Wavelet Transform (HWT) is well suited for increasing the payload and robustness.

Keywords: pixel-wise mask, robust watermark, wavelets, hyper analytic wavelet transform desynchronization attacks

I. INTRODUCTION

The idea of digital watermarking has been proposed as a means to protect the copyright of digital images. However geometric attacks impede the correct detection of the watermark, since the embedder and detector are desynchronized. This is a very serious threat to any real watermarking system, since the attacker does not actually "remove" the watermark, it just hinders the detector. The majority of watermarking algorithms operate based on the spread spectrum (SS) communication principle. A pseudorandom sequence is added to the host image in some critically sampled domain and the watermarked image is obtained by inverse transforming the modified image coefficients. Typical transform domains are the Discrete Wavelet Transform (DWT), the Discrete Cosine Transform (DCT) and the Discrete Fourier Transform (DFT). Numerous Wavelet Transforms (WTs) can be used to embed the watermark. The first one was the DWT, [1]. The DWT based algorithms usually produce watermarked images with the best balance between visual quality and robustness due to the absence of blocking artifacts. It has three main disadvantages, [2]: lack of shift invariance, lack of symmetry of the mother wavelets and poor directional selectivity. Caused by the lack of shift invariance of the DWT, small shifts in the input signal can produce important changes in the energy distribution of the wavelet coefficients. Due to the poor directional selectivity for diagonal features of the DWT the watermarking capacity is small. The most important parameters of a watermarking system are robustness against attacks and capacity. These parameters must be maximized. These disadvantages can be diminished using a complex wavelet transform [2, 3].

In this paper, we present a new technique based on a simple implementation of the hyperanalytic wavelet transform, and compare its performance with two wavelet based methods. We study the resistance of the three multiresolution framework watermarking systems against various signal processing attacks, including the recently proposed local desynchronization attack (DA), namely the local permutation with cancellation and duplication (LPCD) DAs [5].

The paper is organized as follows. In the next two sections, we describe the HWT implementation and the proposed watermarking system in the HWT domain. A section is dedicated to simulation results and finally some remarks are drawn.

I. THE HWT IMPLEMENTATION

If the function ψ is a mother wavelets then the functions $j\mathcal{H}\{\psi\}$ and $\psi_a = \psi + j\mathcal{H}\{\psi\}$ are also mother wavelets, where $\mathcal{H}$ is the Hilbert transform. This wavelet pair $(\psi, j\mathcal{H}\{\psi\})$ defines a complex discrete wavelet transform (CDWT) presented in Fig. 1a). A complex wavelet coefficient is obtained by interpreting the wavelet coefficient from one DWT tree as its real part, whereas the corresponding coefficient from the other tree is imaginary part. The dual tree complex wavelet transform (DT-CWT) [2] is a quadrature pair of DWT trees, similar to the CDWT. The DT-CWT coefficients may be interpreted as arising from the DWT associated with a quasi-analytic wavelet. Both DT-CWT and CDWT are

[1] Faculty of Electronics and Telecommunications, Communications Department
Bd. V. Pârvan Nr. 2, 300223 Timişoara, Romania, e-mail {corina.nafornita, alexandru.isar}@etc.upt.ro

invertible and quasi shift-invariant; however the design of these quadrature wavelet pairs is quite complicated and it can only be done through approximations. The new implementation of the HWT is presented in Fig. 1b). We first apply a Hilbert transform to the data. The real wavelet transform is then applied to the analytical signal associated to the input data, obtaining complex coefficients. The two implementations of the CDWT presented in Fig. 1 are equivalent:

$$\begin{aligned} d_{DTCWT}[m,n] &= \left\langle x(t), \psi_{m,n}(t) + i\mathcal{H}\{\psi_{m,n}(t)\}\right\rangle \\ &= \left\langle x(t), \psi_{m,n}(t)\right\rangle - i\left\langle x(t), \mathcal{H}\{\psi_{m,n}(t)\}\right\rangle \\ &= \left\langle x(t), \psi_{m,n}(t)\right\rangle + i\left\langle \mathcal{H}\{x(t)\}, \psi_{m,n}(t)\right\rangle \\ &= \left\langle x(t) + i\mathcal{H}\{x(t)\}, \psi_{m,n}(t)\right\rangle = d_{HWT}[m,n] \end{aligned} \quad (1)$$

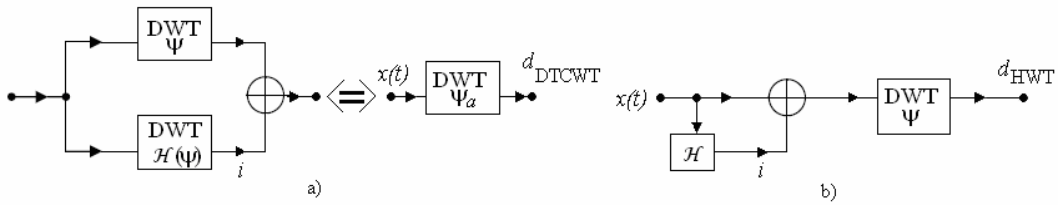

Fig. 1. The implementation of the DT CWT a) and of the HWT b) are equivalent

In fact neither the DT CWT nor the proposed implementation of HWT correspond to perfect analytic mother wavelets, because the exact digital implementation of a Hilbert transform pair of mother wavelets with good performance is not possible in the case of the first transform and because the digital Hilbert transformer is not a realizable system in the case of the second transform. In the following we will use the definition of the analytic signal associated to a 2D real signal named hyper-complex signal. So, the hyper-complex mother wavelet associated to the real mother wavelet $\psi(x,y)$ is defined as:

$$\begin{aligned} &\psi_a(x,y) = \psi(x,y) + i\mathcal{H}_x\{\psi(x,y)\} \\ &+ j\mathcal{H}_y\{\psi(x,y)\} + k\mathcal{H}_x\{\mathcal{H}_y\{\psi(x,y)\}\} \end{aligned} \quad (2)$$

where $i^2 = j^2 = -k^2 = -1$, and $ij = ji = k$, [7]. The HWT of the image $f(x,y)$ is:

$$HWT\{f(x,y)\} = \left\langle f(x,y), \psi_a(x,y)\right\rangle. \quad (3)$$

Taking into account relation (3) it can be written:

$$\begin{aligned} &HWT\{f(x,y)\} \\ &= DWT\{f(x,y)\} + iDWT\{\mathcal{H}_x\{f(x,y)\}\} \\ &+ jDWT\{\mathcal{H}_y\{f(x,y)\}\} + kDWT\{\mathcal{H}_y\{\mathcal{H}_x\{f(x,y)\}\}\} \\ &= \left\langle f_a(x,y), \psi(x,y)\right\rangle = DWT\{f_a(x,y)\}. \end{aligned} \quad (4)$$

The 2D-HWT of the image $f(x,y)$ can be computed with the aid of the 2D-DWT of its associated hyper-complex image.

The new HWT implementation, [6, 8] (fig. 2), uses four trees, each one implementing a 2D-DWT. The first tree is applied to the input image. The second and the third trees are applied to 1D discrete Hilbert transforms computed across the lines ($\mathcal{H}_x$) or columns ($\mathcal{H}_y$) of the input image. The fourth tree is applied to the result obtained after the computation of the two 1D discrete Hilbert transforms of the input image. The enhancement of the directional selectivity of the 2D-HWT is realized as in the case of the 2D-DTCWT, [3, 4], by linear combinations of detail coefficients belonging to each sub-band of each of the four 2D-DWTs. The HWT detail images are oriented following the directions: ±atan(1/2), ±π/4 and ±atan(2). For example, this new implementation makes the difference between the two principal diagonals or between the directions ±atan(1/2) whereas the DWT cannot make such differences.

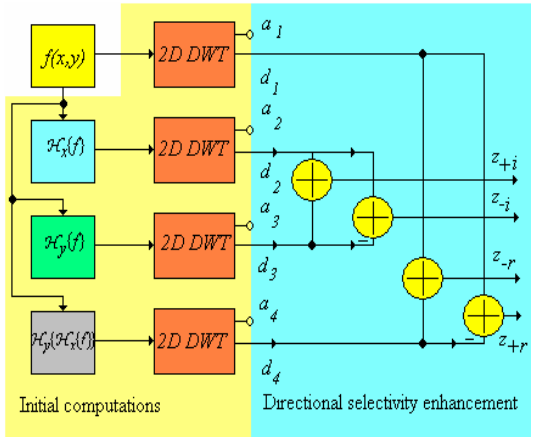

Fig. 2. The new 2D-HWT implementation architecture.

The coefficients z_{+r} and z_{-r} are used in the following simulations for the watermark embeding. A possible representation of the HWT's organization based on these two types of coefficients, that highlights the angles already mentioned, for the first decomposition level, is given in Fig.3a). This structure corresponds to the example in Fig.3b), where the coefficients z_{+r} and z_{-r} of the HWT of the image Lena are represented. It must be mentioned that the sub-images corresponding to the category of coefficients z_{-r} were horizontaly mirrored.

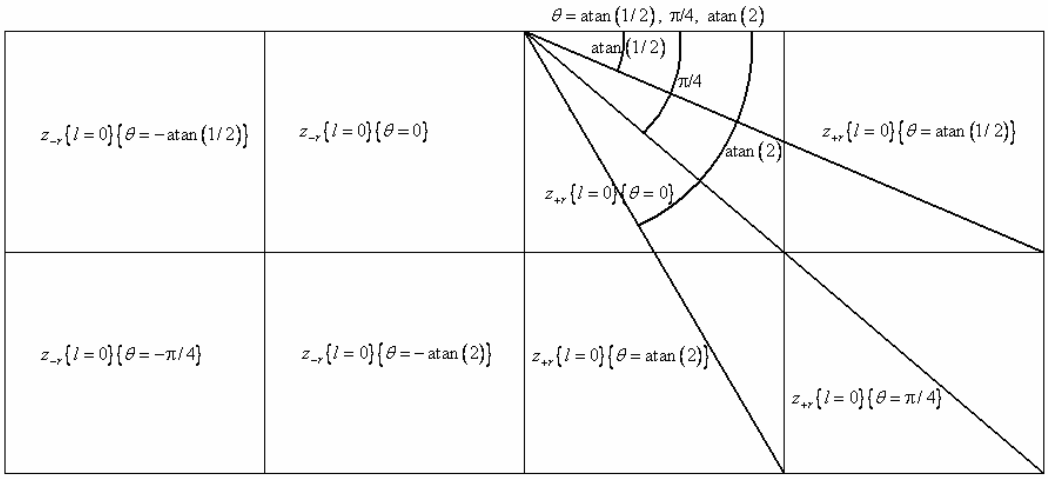

Fig.3a The representation of the real coefficients in which detail sub-images the watermark is embedded.

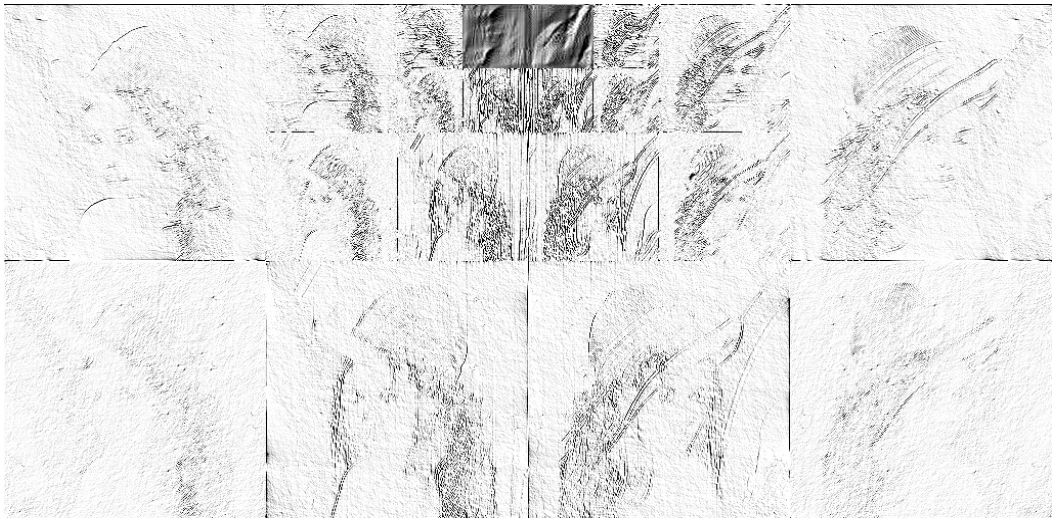

Fig.3b An example for the representation in figure 3a) in the case of the test image Lena, for three levels of decomposition.

III. WATERMARKING BASED ON THE NEW IMPLEMENTATION OF THE HWT

The watermark capacity was studied in [9] where an information-theoretic model for image watermarking and data hiding is presented. Models for geometric attacks and distortion measures that are invariant to such attacks are also considered. The lack of shift invariance of the DWT and its poor directional selectivity are reasons to embed the watermark in the field of another WT. To maximize the robustness and the capacity, the role of the redundancy of the transform used must be highlighted first. An example of redundant WT is represented by the tight frame decomposition. In [10] are analyzed the watermarking systems based on tight frame decompositions. The analysis indicates that a tight frame offers no inherent performance advantage over an orthonormal transform (DWT) in the watermark detection process despite the well known ability of redundant transforms to accommodate greater amounts of added noise for a given distortion. The overcompleteness of the expansion, which aids the watermark insertion by accommodating greater watermark energy for a given distortion, actually hinders the correlation operator in watermark detection. As a result, the tight-frame expansion does not inherently offer greater spread-spectrum watermarking performance. This analytical observation should be tempered with the fact that spread-spectrum watermarking is often deployed in conjunction with an image-adaptive weighting mask to take into account the human visual model (HVM) and to improve perceptual performance. Another redundant WT, the DT-CWT, was already used for watermarking, [11]. The authors of this paper prove that the capacity of a watermarking system based on a complex wavelet transform is higher than the capacity of a similar system that embeds the watermark in the DWT domain. Many authors (e.g. Daugman [12]) have suggested that the processing of visual data inside our visual cortex resembles filtering by an array of Gabor filters of different orientations and scales. We have already proved that the proposed implementation of HWT is efficient, has only a modest amount of redundancy, provides approximate shift invariance, has better directional selectivity than the 2D DWT and it can be observed that the corresponding basis functions closely approximate the

Gabor functions. So, the spread spectrum watermarking based on the use of an image adaptive weighting mask applied in the 2D-HWT domain is potentially a robust solution that increases the capacity. The aim of this paper is to present a new perceptual watermarking technique in the HWT domain. We embed the watermark in the images z_{+r} and z_{-r}, using a perceptual mask; while the blind detection is made on the couple (z_{+r} , z_{-r}). This approach is compared with the classical approach in the DWT domain, from Barni's method [13] and the method proposed in [14].

A. *Perceptual watermarks embedded in the DWT domain*

One of the qualities required to a watermark is its imperceptibility. This can be achieved by embedding the watermark in coefficients of known robustness (usually large coefficients) or perceptually significant regions, i.e. contours and textures of an image. This can be done empirically, selecting larger coefficients or using a thresholding scheme in the transform domain [16,17]. Another approach is to insert the watermark in all coefficients of a transform, using a variable strength for each coefficient [13,14]. Hybrid techniques, based on compression schemes, embed the watermark using a thresholding scheme and variable strength [16]. Specifically we will only refer to the techniques presented in [13] and [14]. The watermark is masked according to the characteristics of the human visual system (HVS), taking into account the texture and the luminance content of all the image subbands [13,14]. For coefficients corresponding to contours of the image a higher strength is used, for textures a medium strength is used and for regions with high regularity a lower strength is used, in accordance with the analogy water-filling and watermarking proposed by Kundur in [15]. Barni's method [13] is quite robust against common signal processing attacks like filtering, compression, cropping etc. However, because embedding is made only in the highest resolution level, the watermark information can be easily erased by a potential attacker. In [14], a new pixel-wise mask was used in the DWT domain that models the HVS behavior in a better way thus allowing embedding of the watermark in all resolution levels, except the last one. At the detection, since the threshold is image dependent, the ratio between correlation and threshold was used; hence the detection function becomes nonlinear with a fixed detection threshold. Three types of detectors are being used, to take advantage of the wavelet hierarchical decomposition. The watermark presence is detected 1) from all resolution levels, 2) separately, considering the maximum detector response from each level and 3) separately, considering the maximum detector response from each subband. Evaluating correlations separately per resolution level or subband is sometimes advantageous. For cropping, the watermark will be damaged more likely in the lower frequency than in the higher frequency, while low-pass filtering affects higher frequency than lower ones. Layers or subbands with lower detector responses are discarded. This type of embedding combined with new detectors is more attack resilient to a possible erasure of the three subbands. At the embedding process [13], the image I, of size $2M\times 2N$, is decomposed into four levels using Daubechies-6 wavelet mother, where I_l^θ is the subband from level $l\in\{0,1,2,3\}$, and orientation $\theta\in\{0,1,2,3\}$ (corresponding to horizontal, diagonal and vertical detail subbands, and approximation subband). A binary watermark $x_l^\theta(i,j)$ is embedded in all coefficients from the subbands from level l by addition

$$\tilde{I}_l^\theta(i,j) = I_l^\theta(i,j) + \alpha w_l^\theta(i,j)\, x_l^\theta(i,j), \qquad (5)$$

where α is the embedding strength and $w_l^\theta(i,j)$ a weighting function. The mask (or equivalently the weighting function) is built pixel by pixel, and it gives the maximum amount of modifications that can be applied to the corresponding DWT coefficient in the detail band without compromising watermark invisibility. This weighting function is a half of the quantization step, which is computed in [13] as the weighted product of three factors:

$$q_l^\theta(i,j) = \Theta(l,\theta)\,\Lambda(l,i,j)\,\Xi(l,i,j)^{0.2}, \qquad (6)$$

and the embedding takes place only in the first level of decomposition, for $l = 0$. The first factor is the sensitivity to noise depending on the orientation and on the level of detail:

$$\Theta(l,\theta) = \begin{Bmatrix} \sqrt{2}, & \theta = 1 \\ 1, & \text{otherwise} \end{Bmatrix} \cdot \begin{Bmatrix} 1.00 & l = 0 \\ 0.32 & l = 1 \\ 0.16 & l = 2 \\ 0.10 & l = 3 \end{Bmatrix} \qquad (7)$$

The second factor takes into account the local brightness based on the gray level values of the low pass version of the image:

$$\Lambda(l,i,j) = 1 + L'(l,i,j), \qquad (8)$$

where

$$L'(l,i,j) = \begin{cases} 1 - L(l,i,j), & L(l,i,j) < 0.5 \\ L(l,i,j), & \text{otherwise} \end{cases}, \qquad (9)$$

and

$$L(l,i,j) = \frac{1}{256} I_3^3\left(1 + \left\lfloor i/2^{3-l} \right\rfloor, 1 + \left\lfloor j/2^{3-l} \right\rfloor\right) \qquad (10)$$

The integer part operator from the right hand side is used to modify the size of the image I_3^3 in accordance with the requirements of the previous decomposition levels. It produces an interpolation of the initial image by multiple repetitions of each row and column. The quality of this procedure degrades rapidly with the

increasing of rows and columns number. The third factor is computed as follows:

$$\Xi(l,i,j)=\sum_{k=0}^{3-l}16^{-k}\sum_{\theta=0}^{2}\sum_{x=0}^{1}\sum_{y=0}^{1}\left[I_{k+l}^{\theta}\left(y+\frac{i}{2^k},x+\frac{j}{2^k}\right)\right]^2 \cdot\mathrm{Var}\left\{I_3^3\left(1+y+\frac{i}{2^{3-l}},1+x+\frac{j}{2^{3-l}}\right)\right\}_{x,y=0,1} \quad (11)$$

and it gives a measure of texture activity in the neighborhood of the pixel. This term is composed by the product of two contributions; the first is the local mean square value of the DWT coefficients in all detail subbands, while the second is the local variance of the low-pass subband. Both these contributions are computed in a small 2×2 neighborhood corresponding to the location (i, j) of the pixel. The first contribution is the distance from the edges, whereas the second one the texture. This local variance estimation is not so precise, because it is computed with a low resolution. In [14], the second factor from Eq. (11) is replaced by the local standard deviation of the image, which has a higher resolution. This is compressed in the wavelet domain to have the same size as the subband where the watermark is to be inserted:

$$\Xi(l,i,j)=\sum_{k=0}^{3-l}16^{-k}\sum_{\theta=0}^{2}\sum_{x=0}^{1}\sum_{y=0}^{1}\left[I_{k+l}^{\theta}\left(y+\frac{i}{2^k},x+\frac{j}{2^k}\right)\right]^2 \cdot\mathrm{DWT}_l^3\left\{\mathrm{Std}(I)_{x,y=0,\ldots,7}\right\} \quad (12)$$

An alternative for the computation of the local mean square value of the DWT coefficients in all detail subbands is to use wavelet interpolation. The second difference between [13] and [14] is that the luminance mask is computed on the approximation image from level l, where the watermark is embedded. The DWT of the original image using l decomposition levels was computed and the approximation sub-image corresponding at level l was separated, obtaining the image I_l^3. Relation (10) was replaced in [14] by:

$$L(l,i,j)=I_l^3(i,j)/256 \quad (13)$$

Since both factors already described are more dependent on the resolution level in the method proposed in [14], the noise sensitivity function is also replaced by:

$$\Theta(l,\theta)=\begin{Bmatrix}\sqrt{2}, & \theta=1\\ 1, & \text{otherwise}\end{Bmatrix}\begin{Bmatrix}1.00 & l\in\{0,1\}\\ 0.66 & l=2\end{Bmatrix} \quad (14)$$

In [13], detection is made using the correlation between the marked DWT coefficients and the watermarking sequence to be tested for presence, for level $l=0$:

$$\rho(l)=\frac{4^l}{3MN}\sum_{\theta=0}^{2}\sum_{i=0}^{M/2^l-1}\sum_{j=0}^{N/2^l-1}\tilde{I}_l^{\theta}(i,j)\,x_l^{\theta}(i,j) \quad (15)$$

The correlation is compared to a threshold $T\rho_{(l)}$, computed to grant a given probability of false positive detection, using the Neyman-Pearson criterion. For example, if $P_f\leq 10^{-8}$, the threshold is $T_{\rho(1)}=3.97\sqrt{\sigma^2_{\rho(1)}}$, with $\sigma^2_{\rho(l)}$ the variance of the wavelet coefficients, if the image was watermarked with a code Y other than X:

$$\sigma^2_{\rho(l)}\approx\left(\frac{4^l}{3MN}\right)^2\sum_{\theta=0}^{2}\sum_{i=0}^{M/2^l-1}\sum_{j=0}^{N/2^l-1}\left(\tilde{I}_l^{\theta}(i,j)\right)^2. \quad (16)$$

In [14] was considered the ratio between the correlation $\rho(l)$ in Eq. (16) and the image dependent threshold $T_{\rho(l)}$, hence the detector was viewed as a nonlinear function with a fixed threshold. Three detectors are being used. The first detector evaluates the watermark's presence on all resolution levels:

$$d_1=\rho_{d1}/T_{d1} \quad (17)$$

where the correlation ρ_{d1} is given by:

$$\rho_{d1}=\frac{1}{3MN\sum_{l=0}^{2}4^{-l}}\sum_{l,\theta==0}^{2}\sum_{i=0}^{M/2^l-1}\sum_{j=0}^{N/2^l-1}\tilde{I}_l^{\theta}(i,j)\,x_l^{\theta}(i,j) \quad (18)$$

The threshold for $P_f\leq 10^{-8}$ is $T_{\mathrm{d1}}=3.97\sqrt{\sigma^2_{\rho\mathrm{d1}}}$, with:

$$\sigma^2_{\rho\mathrm{d1}}\approx\frac{1}{\left(3MN\sum_{l=0}^{2}4^{-l}\right)^2}\sum_{l,\theta=0}^{2}\sum_{i,j=0}^{M/2^l-1,\,N/2^l-1}\left(\tilde{I}_l^{\theta}(i,j)\right)^2 \quad (19)$$

The second detector considers the responses from different levels, as $d(l)=\rho(l)/T\rho_{(l)}$, with $l\in\{0,1,2\}$, and discards the detector responses with lower values:

$$d_2=\max_l\{d(l)\} \quad (20)$$

The third detector considers the responses from different subbands and levels, as $d(l,\theta)=\rho(l,\theta)/T(l,\theta)$, with $l,\ \theta\in\{0,1,2\}$, and discards the detector responses with lower values:

$$d_3=\max_{l,\theta}\{d(l,\theta)\} \quad (21)$$

where $\rho(l,\theta)$ and $T(l,\theta)$ are the correlations and thresholds for each subband. For $P_f\leq 10^{-8}$, the threshold is $T(l,\theta)=3.97\sqrt{\sigma^2_{\rho(l,\theta)}}$, with $\sigma^2_{\rho(l,\theta)}$ the variance of wavelet coefficients from the subband (l,θ):

$$\rho(l,\theta)=4^l\sum_{i=0}^{M/2^l-1}\sum_{j=0}^{N/2^l-1}\tilde{I}_l^{\theta}(i,j)\,x_l^{\theta}(i,j)\Big/(MN) \quad (22)$$

and

$$\sigma^2_{\rho(l,\theta)}\approx 16^l\sum_{i=0}^{M/2^l-1}\sum_{j=0}^{N/2^l-1}\left(\tilde{I}_l^{\theta}(i,j)\right)^2\Big/(MN)^2 \quad (23)$$

B. *Perceptual watermarks embedded in the HWT domain*

Adapting the strategy already described in the previous paragraph to the case of HWT, we have decided to use the first three wavelet decomposition levels. We have embedded the watermark into the coefficients z_{+r} and z_{-r}. In this case the relations already described in the previous paragraph were used independently for each of these two images. The same message was embedded in both images, using the mask from [14]. The difference is that the orientations or preferential directions are in this case: atan(1/2), π/4, atan(2) (respectively for θ = 0,1,2), for the image z_{+r} and -atan(1/2), -π/4, -atan(2), (θ=0,1,2) for the image z_{-r}. At the detection side, we consider the pair of images (z_{+r}, z_{-r}), thus having twice as much coefficients than the standard approach, and θ takes all the possible values, ±atan(1/2), ±π/4, ±atan(2).

IV. SIMULATION RESULTS

Some simulation results, obtained using the image Lena, of size 512x512, are reported in the following. For α = 1.5, and a watermark inserted in all levels: 0, 1 and 2, the image watermarked in the HWT domain has a peak signal-to-noise ratio (PSNR) of 35.63 dB, and a weighted PSNR of 52 dB (see table 1).
The peak signal-to-noise ratio, PSNR is defined as:

$$PSNR\left(I,\tilde{I}\right)=10\log_{10}\left[\frac{255^2}{\frac{1}{N}\sum_i\left(\tilde{I}_i-I_i\right)^2}\right]\ [\text{dB}]$$

where I is the host signal, $\tilde{I}$ is the watermarked signal, i is the particular pixel position, and N is the number of pixels in I or $\tilde{I}$. Another measure is the weighted PSNR (WPSNR); where weighting is performed according to the contrast sensitivity function, CSF, of vision as defined in [18].

The original image, the corresponding watermarked image and the difference image are presented in Fig. 4. We have exposed our watermarked images at some common attacks: JPEG compression with different quality factors (Q), shifting, median filtering with different window sizes M, resizing with different scale factors, cropping with different areas remaining, gamma correction with different values of γ, blurring with a specified point spread function (PSF) and perturbation with AWGN with different variances and we have studied the robustness of the new watermarking method. The PSF is specified with the aid of two parameters: length L and angle β. Resistance to unintentional attacks, for watermarked image Lena, for our new method, can be compared to the results obtained using the watermarking methods reported in [13] and [14] analyzing table 2. In the simulation corresponding to the watermarking method proposed in [14], we use the same watermark strength, 1.5 and we embed the watermark in all three wavelet decomposition levels, resulting in a PSNR of 36.86 dB and a weighted PSNR of 53.20 dB. For the simulation corresponding to the watermarking method proposed in [13], we use the watermark strength 0.2 and the embedding is made only in the first resolution level, resulting in a similar quality of the images in terms of classical PSNR value (PSNR=36.39 dB, weighted PSNR=33.20 dB).

Special attention was paid to the shifting attack. First the watermarked image was circularly shifted with *li* lines and *co* columns, obtaining the attacked image $\left(\tilde{I}_t\right)$. Supposing that the numbers *li* and *co* are known, the messages at level *l* are circularly shifted with $li/2^l$ lines and $co/2^l$ columns obtaining the new messages $\left(x_t\right)_l^{\theta}$. Next the watermark was detected using the image $\left(\tilde{I}\right)_t$ and the messages $\left(x_t\right)_l^{\theta}$. The values obtained for *li*=128 and *co*=128 are presented in table 2. From the results, it is clear that embedding in the real parts of the HWT transform yields in a higher capacity at the same visual impact and robustness. In fact the results obtained for the new method are slightly better than the results obtained with the methods described in [13] and [14] for JPEG compression, median filtering with window size M=3, resizing and gamma correction. For the other attacks the results obtained using the new method are similar with the results of the watermarking methods based on DWT. The case of the shifting attack is very interesting. In this case the robustness of the watermarking method is given by two properties: the shift invariance degree of the WT used and the masking ability. All the methods compared in table 2 are very robust against the shifting attack. The values of the ratios between the correlations and the image dependent thresholds obtained before and after the shifting attack are equal for all the methods compared in table 2. So, the ability of masking seems to be more important than the shift invariance degree of the WT used for the conception of counter-measures against the shifting attack, when the numbers of lines and columns used for the attack are already known. Of course, the detection of these numbers must also be realized, for the implementation of a strategy against the shifting attack. So, the shift invariance of the real values of the HWT coefficients is very good, and the watermark can be detected despite this attack for a large variety of lines and columns numbers. Next, we have submitted the watermarked images to the recently proposed local desynchronization attack (DA), namely the local permutation with cancellation and duplication (LPCD) DAs [5]. The parameters used in the attack were the ones that visually damage the image less indicated by the authors, N=5 and L=6. The watermark is successfully detected each time, for each method.

Fig. 4. Original and watermarked images with the new method, for $\alpha = 1.5$, PSNR=35.63 dB; Difference image, amplified 8 times.

Table 1. Comparison of invisibility for the proposed method and the traditional approaches [13], [14]

Measure of invisibility vs. methods	Method proposed in [14]	Barni's method [13]	Proposed HWT method
PSNR	36.86 dB	36.39 dB	35.60 dB
Weighted PSNR	53.20 dB	33.20 dB	52.00 dB

Table 2. Comparison of robustness for different unintentional attacks. The HWT method proposed here, as well as the traditional approaches from [13] and [14] are compared.

Attacks vs. detector response	Method proposed in [14]			Barni's method [13]	Proposed HWT method		
	all levels	max level	max subband		all levels	max level	max subband
Before attack	21.57	39.12	33.60	**44.31**	24.78	43.18	26.30
JPEG, Q=50	5.45	6.76	5.02	6.22	6.25	**7.87**	4.85
JPEG, Q=25	3.02	3.67	2.60	3.03	3.23	**4.19**	2.62
JPEG, Q=20	2.55	3.08	2.09	2.38	2.72	**3.58**	2.33
Shift, *li*=128, *co*=128	21.57	39.12	33.59	**44.31**	24.78	43.18	26.30
Median filtering, M=3	4.29	4.58	4.87	1.57	4.59	**5.42**	4.37
Median filtering, M=5	**1.66**	1.24	2.27	0.59	1.61	1.64	1.49
Resizing, 0.75	9.53	15.86	15.64	14.09	10.93	**19.34**	14.67
Resizing, 0.50	4.21	5.72	5.75	2.31	4.56	6.14	**8.71**
Cropping, 256x256	7.40	12.14	17.10	**18.08**	8.68	15.20	13.82
Cropping, 128x128	3.11	4.66	**8.31**	8.01	3.53	6.04	6.86
Cropping, 64x64	1.10	1.72	**4.45**	3.92	1.32	2.47	3.71
Gamma correction, γ=1.5	22.18	39.76	33.74	43.04	25.31	**43.61**	26.45
Gamma correction, γ=2	22.59	39.70	32.98	42.43	25.62	**43.24**	25.88
Blur, L=31, β=11	2.69	7.81	**9.56**	9.05	3.05	9.18	7.55
LPCD attack, N=5.L=6	9.99	16.13	15.33	**24.84**	12.23	19.58	12.34

Fig. 5: (*left*) Watermarked image for the method in [14], having a PSNR=36.86 dB and a weighted PSNR=53.20 dB compared to the original Lena, (*middle*) Distorted watermarked with the LPCD attack N=5 and L=6 with PSNR=29.20 dB, weighted PSNR=38.41 dB, (right) Difference between the two images, magnified 100 times

Fig. 6: (*left*) Watermarked image for Barni's method [13], having a PSNR=36.39 dB and a weighted PSNR=33.20 dB compared to the original Lena, (*middle*) Distorted watermarked with the LPCD attack N=5 and L=6 with PSNR=30.68 dB, weighted PSNR=30.82 dB, (right) Difference between the two images, magnified 100 times

Fig. 7: (*left*) Watermarked image for the HWT based method, having a PSNR=35.60 dB and a weighted PSNR=52 dB compared to the original Lena, (*middle*) Distorted watermarked with the LPCD attack N=5 and L=6 with PSNR=28.16 dB, weighted PSNR=37.87 dB, (right) Difference between the two images, magnified 100 times

IV. CONCLUSION

The HWT is a very modern WT as it has been formalized only two years ago. In this paper we have used a very simple implementation of this transform, which permits the exploitation of the mathematical results and of the algorithms previously obtained in the evolution of wavelets theory. It does not require the construction of any special wavelet filter. It has a very flexible structure, as we can use any orthogonal or bi-orthogonal real mother wavelets for the computation of the HWT. The proposed implementation leads to both a high degree of shift-invariance and to an enhanced directional selectivity in the 2D case. In the theoretical derivations reported in this paper we have considered an ideal Hilbert transformer.

We have proposed a new type of pixel-wise masking for robust image watermarking in the HWT domain. Modifications were made to two existing watermarking technique proposed in [13] and in [14], based on DWT. These techniques were selected for their good robustness against the usual attacks. The method proposed in [14] was inspired by the method proposed in [13], but it contains some modifications. The first modification is in computing the estimate of

the variance, which gives a better measure of the texture activity. An improvement is also owed to the use of a better luminance mask. The third improvement proposed in [14] is to embed the watermark in the detail coefficients at all resolutions, except the coarsest level; this can be particularly useful against erasure of high frequency subbands containing the mark in the watermarking system proposed in [13]. A nonlinear detector with fixed threshold – as ratio between correlation and the image dependent threshold-has been conceived. Using it, three watermark detectors were proposed in [14]: 1) from all resolution levels, 2) separately, considering the maximum detector response for each level and 3) separately, considering the maximum detector response for each subband. A HWT embedding mechanism is proposed, exploiting the coefficients z_{+r} and z_{-r}.

The simulation results presented in this paper illustrate the effectiveness of the proposed algorithm. We tested the robustness of our method against different attacks, and found out that it is similar or better than the robustness of the methods described in [30] and [31] in the case of the image Lena.

Our watermarking method has superior capacity than the method proposed in [13] and even [14].

REFERENCES

[1] D. L. Donoho, I. M. Johnstone, "Ideal spatial adaptation by wavelet shrinkage", *Biometrika*, 81(3) : 425-455, 1994.

[2] N. Kingsbury, "Complex Wavelets for Shift Invariant Analysis and Filtering of Signals", *Applied and Comp. Harm. Anal.* 10, '01, 234-253.

[3] N. G. Kingsbury, "A Dual-Tree Complex Wavelet Transform with improved orthogonality and symmetry properties", *Proc. IEEE Conf. on Image Processing*, Vancouver, '00, paper 1429.

[4] I. W. Selesnick, R. G. Baraniuk, and N. G. Kingsbury, "The dual-tree complex wavelet transform", *IEEE Signal Processing Magazine*, vol. 22(6), '05, 123–151.

[5] Angela D'Angelo, Mauro Barni, and Neri Merhav, "Stochastic Image Warping for Improved Watermark Desynchronization," EURASIP Journal on Information Security, vol. 2008, Article ID 345184, 14 pages, 2008.

[6] I. Adam, C. Nafornita, J-M Boucher, A. Isar, "A New Implementation of the Hyperanalytic Wavelet Transform", Proc. of IEEE Symposium *ISSCS 2007*, Iasi, Romania, '07, 401-404.

[7] C. Davenport, "Commutative Hypercomplex Mathematics", http://home.usit.net/~cmdaven/cmdaven1.htm

[8] I. Adam, C. Nafornita, J.-M. Boucher and A. Isar, "A Bayesian Approach of Hyperanalytic Wavelet Transform Based Denoising", Proc. *IEEE International Conference WISP'07*, Alcala de Henares, Spain, '07, 237-242.

[9] Pierre Moulin and M. Kivanc Mihcak, "A Framework for Evaluating the Data-Hiding Capacity of Image Sources", *IEEE Trans. Image Processing*, 11(9), '02, 1029-1042.

[10] Li Hua and James E. Fowler, "A Performance Analysis of Spread-Spectrum Watermarking Based on Redundant Transforms", Proc. IEEE *Int. Conf. on Multimedia and Expo*, Lausanne, Switzerland, '02, vol. 2, 553–556.

[11] Patrick Loo, Nick Kingsbury, "Digital Watermarking Using Complex Wavelets", *ICIP 2000*.

[12] J. Daugman, "Two-dimensional spectral analysis of cortical receptive field profiles", *Vision Res.*, 20, '80, 847-856.

[13] M. Barni, F. Bartolini and A. Piva, "Improved wavelet-based watermarking through pixel-wise masking", *IEEE Trans. Image Processing*, 10, '01, 783-791.

[14] C. Nafornita, "A New Pixel-Wise Mask for Watermarking", Proc. *ACM Multimedia and Security MM&Sec*, Dallas, Sept '07, 221-228.

[15] D. Kundur, "Water-filling for Watermarking?" *Proc. IEEE Int. Conf. Multimedia and Expo*, NY, '00, 1287-1290.

[16] C. Podilchuk and W. Zeng, "Image-Adaptive Watermarking Using Visual Models", *IEEE Journal on Selected Areas in Communications*, 16, 4, May 1998, 525-539.

[17] C. Nafornita, C., A. Isar and M. Borda, "Image Watermarking Based on the Discrete Wavelet Transform Statistical Characteristics", Proc. *IEEE EUROCON 2005*, Serbia & Montenegro, 943-946.

[18] Miyahara, M.; Kotani, K.; Algazi, V.R., "Objective Picture Quality Scale (PQS) for Image Coding", *IEEE Trans. on Comm.*, Vol 46, No.9, 1998.